concentration using a Varian CP-3800 gas chromatograph with a thermal conductivity detector. Rates of CO_2 production were calculated by dividing concentrations by the time since jars had been sealed. On the same date, we collected samples of gas from the headspace of incubation jars for determining the $\delta^{13}C$ value of the accumulated CO_2. We injected 7 ml of headspace gas into He-flushed gas-tight LabCo exetainers, which were then placed into an autosampler and analysed on a FIN-MAT Gas Bench II connected to the IRMS. Soil respiration $\delta^{13}C$ values for control and elevated O_3 treatments were -25.0 ± 0.2‰ across the incubation. For soils from elevated CO_2, soil respiration values initially were -30.9 ± 0.3‰ and increased to -28.8 ± 0.2‰ by day 281 of incubation. For the elevated $O_3 + CO_2$ treatment, values initially were -31.1 ± 0.4‰ and -28.2 ± 0.2 at day 281 of incubation.

Stable isotope tracer, calculations and statistical analysis

To investigate the contribution of new carbon inputs to soil and microbial respiration in the elevated CO_2 and elevated $O_3 + CO_2$ plots, we used the $\delta^{13}C$ signature derived from the fossil-fuel fumigation gas mixed with ambient air (-18.7 ± 1.0‰ compared to -8.6 ± 0.1‰ for control and elevated O_3 plots). Subsequent fractionation by the plants produced leaf and root tissue with $\delta^{13}C$ values of approximately -41.6 ± 0.4‰ in elevated CO_2 and elevated $O_3 + CO_2$ plots. Composite soil samples collected from all 12 plots before the experiment began in 1997 and from the three control plots in 2001 had similar ($P = 0.47$) $\delta^{13}C$ values, averaging -26.7 ± 0.2‰. The proportional contribution of carbon derived from the fumigation gas (f) was calculated using the equation $f = (\delta_t - \delta_o)/(\delta_i - \delta_o)$, where δ_t refers to the isotopic composition ($\delta^{13}C$) of the soil organic carbon or soil respiration from the fumigated (elevated CO_2 or elevated $O_3 + CO_2$) plots, δ_o is the $\delta^{13}C$ of soil organic carbon or soil respiration from control plots, and δ_i is the ^{13}C signature of the plant leaves and roots collected in 2001 from the fumigated plots, weighted equally and averaged across species as there were no significant differences found among the aspen and aspen–birch plots. We do not expect that the isotopic signature of the plants varied appreciably over the life of this experiment because fumigation was initiated when the trees were still seedlings. Because there were differences among treatments in the amount of carbon entering soils derived from fumigation (Fig. 1), we calculated the relative mass loss as the cumulative amount of carbon respired from each of these pools divided by the amount of soil carbon in that pool. Data were analysed using analysis of variance with general linear models for a split-plot randomized complete design using SAS 8.02 (Cary, North Carolina).

1. *IPCC Climate Change 2001: Technical Summary* (Report of the Intergovernmental Panel on Climate Change, IPCC Secretariat, Geneva, 2001).
2. Gregg, J. W., Jones, C. G. & Dawson, T. E. Urbanization effects on tree growth in the vicinity of New York City. *Nature* **424**, 183–187 (2003).
3. McLaughlin, S. B. & Downing, D. J. Interactive effects of ambient ozone and climate measured on growth of mature forest trees. *Nature* **374**, 252–254 (1995).
4. Chameides, W. L., Kasibhatla, P. S., Yienger, J. & Levy, H. I. Growth of continental-scale metro-agro-plexes, regional ozone pollution, and world food production. *Science* **264**, 74–77 (1994).
5. Percy, K. E. *et al.* Altered performance of forest pests under CO_2- and O_3-enriched atmospheres. *Nature* **420**, 403–407 (2002).
6. *Latest Findings on National Air Quality: 2002 Status and Trends* (US Environmental Protection Agency).
7. Findlay, S., Carreiro, M., Krischik, V. & Jones, C. G. Effects of damage to living plants on leaf litter quality. *Ecol. Appl.* **6**, 269–275 (1996).
8. Coleman, M. D., Dickson, R. E., Isebrands, J. G. & Karnosky, D. F. Carbon allocation and partitioning in aspen clones varying in sensitivity to tropospheric ozone. *Tree Physiol.* **15**, 593–604 (1995).
9. Andersen, C. P. Source-sink balance and carbon allocation below ground in plants exposed to ozone. *New Phytol.* **157**, 213–228 (2003).
10. King, J. S. *et al.* Fine-root biomass and fluxes of soil carbon in young stands of paper birch and trembling aspen as affected by elevated atmospheric CO_2 and tropospheric O_3. *Oecologia* **128**, 237–250 (2001).
11. Dickson, R. E. *et al.* Forest Atmosphere Carbon Transfer and Storage (FACTS-II)—The Aspen Free-air CO_2 and O_3 Enrichment (FACE) Project: An Overview (Technical Report NC-214, USDA, Washington DC, 2000).
12. Leavitt, S. W., Follett, R. F. & Paul, E. A. Estimation of slow- and fast-cycling soil organic carbon pools from 6N HCl hydrolysis. *Radiocarbon* **38**, 231–239 (1996).
13. Paul, E. A. *et al.* Radiocarbon dating for determination of soil organic matter pool sizes and dynamics. *Soil Sci. Soc. Am. J.* **61**, 1058–1067 (1997).
14. Phillips, R., Zak, D. R., Holmes, W. E. & White, D. C. Microbial community composition and function beneath temperate trees exposed to elevated atmospheric carbon dioxide and ozone. *Oecologia* **131**, 236–244 (2002).
15. Larson, J., Zak, D. R. & Sinsabaugh, R. L. Extracellular enzyme activity beneath temperate trees growing under elevated carbon dioxide and ozone. *Soil Sci. Soc. Am. J.* **66**, 1848–1856 (2002).

Competing interests statement The authors declare that they have no competing financial interests.

Correspondence and requests for materials should be addressed to W.M.L. (wmloya@mtu.edu).

Flying and swimming animals cruise at a Strouhal number tuned for high power efficiency

Graham K. Taylor, Robert L. Nudds* & Adrian L. R. Thomas

Zoology Department, University of Oxford, Tinbergen Building, South Parks Road, Oxford OX1 3PS, UK

* Present address: School of Biology, University of Leeds, L. C. Miall Building, Clarendon Way, Leeds LS2 9JT, UK

Dimensionless numbers are important in biomechanics because their constancy can imply dynamic similarity between systems, despite possible differences in medium or scale[1]. A dimensionless parameter that describes the tail or wing kinematics of swimming and flying animals is the Strouhal number[1], $St = fA/U$, which divides stroke frequency (f) and amplitude (A) by forward speed (U)[2–8]. St is known to govern a well-defined series of vortex growth and shedding regimes for airfoils undergoing pitching and heaving motions[6,8]. Propulsive efficiency is high over a narrow range of St and usually peaks within the interval $0.2 < St < 0.4$ (refs 3–8). Because natural selection is likely to tune animals for high propulsive efficiency, we expect it to constrain the range of St that animals use. This seems to be true for dolphins[2–5], sharks[3–5] and bony fish[3–5], which swim at $0.2 < St < 0.4$. Here we show that birds, bats and insects also converge on the same narrow range of St, but only when cruising. Tuning cruise kinematics to optimize St therefore seems to be a general principle of oscillatory lift-based propulsion.

Experiments with isolated pitching or heaving foils have measured extremely high peak propulsive efficiencies within the interval $0.2 < St < 0.4$ (modal peak at $St \approx 0.3$)[3–7]. In this range, the propulsive efficiency (defined as the ratio of aerodynamic power output to mechanical power input) can be as high as 70% (ref. 7) or even 80% (ref. 6). Optimal St depends subtly on kinematic parameters including geometric angle of attack, amplitude-to-chord ratio, airfoil section and phase of motion[6–8] but, for any given motion, efficiency is usually high ($>60\%$) over a range narrower than $0.2 < St < 0.4$ (refs 3–7). For example, measured efficiency can plummet from 80% at $St = 0.27$ to 10% at $St = 0.09$ (ref. 6) and also drops off at higher St, albeit more gently[7,8]. Measured propulsive efficiency usually peaks when the kinematics result in maximum amplification of the shed vortices in the wake and an average velocity profile equivalent to a jet[3,4,6].

Theoretical treatments of flapping wings[3,4,6,8] further confirm the empirical result that St tightly constrains propulsive efficiency. In fact, St is bound to affect aerodynamic force coefficients and propulsive efficiency, because it defines the maximum aerodynamic angle of attack and the timescales associated with the growth and shedding of vortices, which are the source of aerodynamic force production[8,9]. Natural selection is expected to favour wing kinematics that combine high propulsive efficiency with a high aerodynamic force coefficient. These need not peak at identical St, but can do for certain motions[7,8]; if not, selection should optimize the trade-off. Propulsive efficiency may be the more important selection pressure in cruising, whereas high aerodynamic force coefficients may be more important in accelerations, slow locomotion or hovering. In cruising flight or swimming, we therefore predict that St will be tuned for high propulsive efficiency.

This suggestion has already been made for cruising fish and dolphins[2–5], which operate within the range $0.2 < St < 0.4$, and the principle is considered so general for swimming animals that it has even been used to predict the speeds of extinct ichthyosaurs[10]. Whereas the fluid dynamic results described above[3–8] refer to

isolated flapping foils, swimming animals usually beat their tail in the wake of their own body. Non-streamlined bodies shed vortices at a natural frequency (also defined by a Strouhal number), which the tail can tune into to regain energy lost into the wake[5,11–13]. As this will complicate selection of St, swimming animals may be less well modelled by isolated flapping foils than are flying animals (whose wings do not operate in their body's wake, thereby avoiding competition between a natural and a forced shedding mode). Similar complications may arise where favourable interactions occur between the wings and wake following stroke reversal, or where the fore and hind wings interact. This will be especially problematic in slow-flying insects, and may be important for insects generally, but the paucity of kinematic data for cruising insects makes this difficult to test.

The results for isolated flapping foils consider only pitching and heaving motions, such as those used by swimming animals[3–8]. The root-flapping motions of flying animals seem not to have been tested. We therefore subjected a hinged flat plate to heaving or root-flapping motions to check whether these motions induced the same vortex growth and shedding regimes at similar St. We equate stroke amplitude with wingtip excursion, which makes sense because the wake is bounded by vorticity shed at the wingtips and the aerodynamics are dominated by the faster-moving outboard wing elements. This simple definition is also directly equivalent in

heaving, pitching and root-flapping motions. We found that heaving generated larger vortices than root-flapping (presumably because average velocity was higher across the span), but otherwise the same four distinct wake regimes occurred at similar St (Fig. 1). By analogy with swimming animals, we therefore predicted that flying animals would have been selected to operate in the same range $0.2 < St < 0.4$ for efficient cruising.

To test this prediction, we identified 16 studies that reported wingbeat frequency, stroke amplitude and flight speed[14–29] in steady cruising flight. All of the analysis was done with Matlab 6.5. If wingtip excursion A was not directly measured, we approximated A as $A \approx b\sin\theta/2$, where b is span and θ is dorsoventral stroke angle. This allowed us to calculate St for 42 species (Fig. 2) from 14 bird ($n = 22$), 6 bat ($n = 18$) and 2 insect ($n = 2$) families. Insect flight research has tended to focus on slow or hovering flight, and further data on cruising insects are clearly required before generalizing to other insects, especially as cruising power efficiency may not be a strong selection pressure in many species. In most cases, we used mean or modal values collected from animals flying naturally in the wild. In wind tunnel studies in which the animal was forced to fly at pre-determined speeds, St was calculated for the reported preferred flying speed[22,23,26,27]. We excluded studies in which the animal was otherwise confined and liable to be flying slowly.

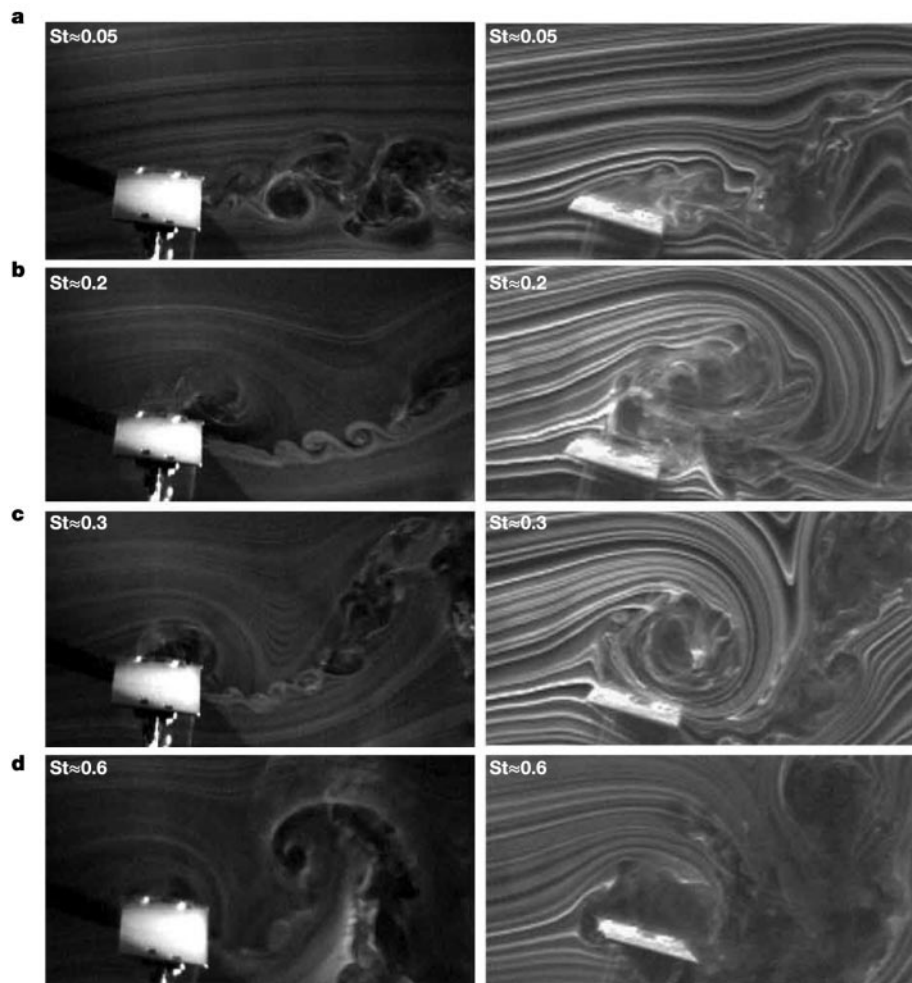Figure 2 clearly shows that swimming and flying animals all

Figure 1 Wake structures for root-flapping and heaving hinged flat plates at varying St. Left panels, root-flapping motion; right panels, heaving motion. Amplitude, twice wing chord; static angle of attack, 15°; flow speed, 1.5 ms^{-1}; smoke wire visualizations made at end of downstroke. **a**, For St < 0.10, flow separates at the sharp leading-edge, but no discrete vortex forms. **b**, For $0.10 < St < 0.25$, a leading-edge vortex forms but is shed before the downstroke ends. **c**, For $0.25 < St < 0.45$, the leading-edge vortex is shed as the downstroke ends. **d**, For St > 0.45, trailing edge separation produces a characteristic mushroom-shaped wake. At higher St, the wing collides with shed vorticity on the upstroke, giving an energetically inefficient mode.

operate at similar St. Does this reflect selection to constrain St, or is it merely coincidental? To answer this, we first provide two independent confirmations that St is tightly constrained in cruising flight. The first confirmation comes from considering how St varies when an animal is forced to fly other than at its preferred speed. St varies more in four individual zebra finches (*Taenopygia guttata*)[27] forced to fly between 4 and 14 ms^{-1} than across all 42 species flying at their preferred speeds (Fig. 2). Even excluding the lowest forced flight speeds (which are lower than any preferred flight speed), the standard deviation (s.d.) of St for the zebra finch across speeds is more than twice that for all 42 species flying at their preferred speeds. Flight speed affects St so strongly because wingbeat frequency and amplitude are tightly constrained, presumably by physiology and morphology. This makes it even more notable that, when only cruise performance is considered, a sample spanning five orders of body mass and three independent evolutionary origins of flight shows less than half the variation in St found in four individuals of a single species forced to fly at different speeds.

A Monte Carlo analysis provides a second confirmation that St is tightly constrained in cruising flight (Fig. 3). As frequency, speed and amplitude all scale with body mass (m), if wing kinematics are indeed tuned to optimize St, their residual variation should co-vary appropriately to constrain St. We therefore regressed $\log(f)$, $\log(U)$ and $\log(A)$ separately against $\log(m)$ and calculated the fitted values for each species. We then randomly allocated 1 of the 42 residuals from each of the regressions to each species without replacement and calculated the s.d. of St in the resulting sample ($n = 42$). We repeated this procedure 50,000 times.

Figure 3 shows the distribution of the s.d. of resampled St. Regressions and residual plots (Supplementary Fig. S1) showed sufficient homoscedasticity for the procedure to be valid. Only 53 of the 50,000 randomized combinations of residuals ($<0.11\%$) had a lower s.d. of St than the original sample. The actual s.d. of St (0.10) was therefore significantly smaller than expected by chance ($P = 0.001$) from the allometry of f, U and A. This is very strong evidence that St is tightly constrained during cruising flight. It would not be unexpected to find St tightly constrained in similar species, because similar morphological and physiological constraints usually produce dynamic similarity[1]; however, it is surprising to find St tightly constrained in this morphologically and physiologically disparate sample, unless St is constrained by one uniting factor—aerodynamics.

The propulsive efficiency of an isolated flapping foil usually peaks at St ≈ 0.3 (refs 3–7), therefore we used a two-tailed t-test to check that actual mean St = 0.29 did not differ significantly ($P = 0.136$) from this (after square-root transforming the data to remove skew arising because St is a ratio). The data are not normally distributed even after transformation (Supplementary Fig. S2), but the t-test is robust to large deviations from normality and, as the 95% confidence interval ($0.25 < $ St $ < 0.31$) fell comfortably inside the optimal range $0.2 < $ St $ < 0.4$, we can be reasonably sure that the lack of any statistically significant difference is not merely an artefact of low statistical power. Median St = 0.25 (inter-quartile range 0.20–0.35) was less than mean St because of the positive skew, but still did not differ significantly from the expected optimum (sign test, $P = 0.081$). St therefore seems to have converged on the expected optimum St ≈ 0.3 in cruising flight, with about 75% of species falling in the range $0.19 < $ St $ < 0.41$. In addition, the fit is remarkably tight given the much larger variation in St found in a single species forced to fly at different speeds.

Because the assumptions of parametric analysis of variance are unlikely to hold for our data set, we used a Kruskal–Wallis test to compare St among taxonomic classes. The test just failed to attain statistical significance ($P = 0.054$), mainly because the $n = 2$ sample size for insects limited its efficiency. Using a Wilcoxon rank sum test to compare directly birds and bats showed instead that St is significantly lower in birds than in bats (two-tailed, $P = 0.020$). We then dropped all families of $n = 1$ and used a
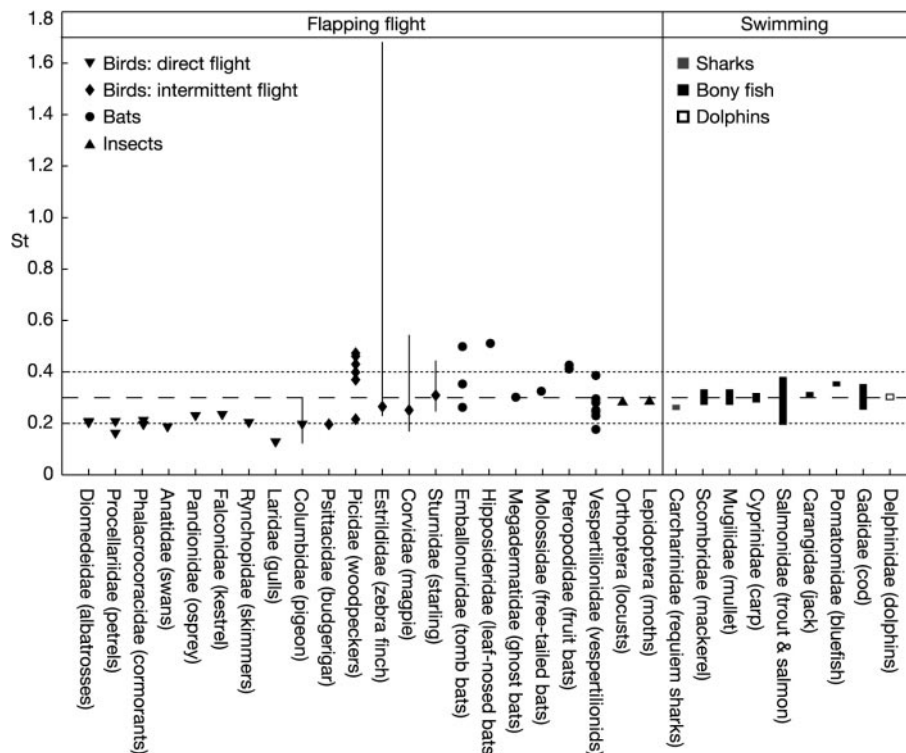

Figure 2 Strouhal number for 42 species of birds, bats and insects in unconfined, cruising flight. Published ranges[3,4] of St in cruising fish and dolphins are included for comparison. Dotted lines mark the range $0.2 < $ St $ < 0.4$, in which propulsive efficiency usually peaks; dashed line marks the modal peak at St = 0.3. Unbroken lines indicate the range of variation in St across other non-zero flight speeds, where such data exist.
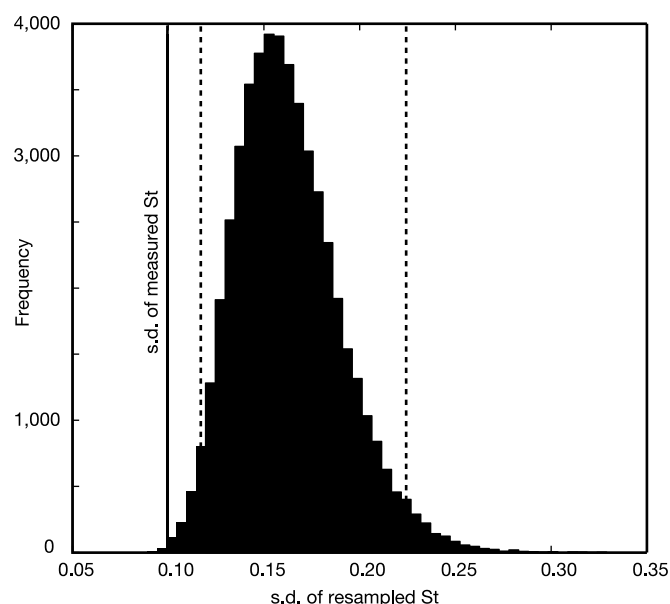
Figure 3 Histogram from Monte Carlo analysis recalculating St for 50,000 iterations randomizing the order of residuals from regressing log(f), log(U) and log(A) against log(m). Dotted lines denote the 95% confidence interval for the s.d. of the sample expected by chance from the regressions; the actual s.d. was significantly less than expected by chance ($P = 0.001$).

Kruskal–Wallis test to look for interfamilial variation within birds and bats. St varied significantly between the four remaining bird (two-tailed $P = 0.036$) and the three remaining bat (two-tailed, $P = 0.032$) families. *A posteriori* comparisons between the mean ranks using Tukey's honestly significant difference procedure ($\alpha = 0.05$) were too conservative to identify which differences were significant (the procedure forfeits sensitivity for individual differences to control the overall risk of type I error). We therefore used Tukey's least significant difference procedure ($\alpha = 0.05$), which is more liberal but indicated that St was significantly higher for woodpeckers than for petrels, and significantly lower for vespertilionid bats than for fruit bats.

Birds using intermittent flight (median St = 0.34, inter-quartile range 0.25–0.43, $n = 10$) have significantly higher St (Wilcoxon rank sum test, $P < 0.001$) than birds using direct flight (median St = 0.20, inter-quartile range 0.19–0.21, $n = 12$). Direct fliers occupy the lower extreme of the range $0.2 < St < 0.4$ (Fig. 2), where leading-edge separation is weak or non-existent for classical airfoils[6]. Intermittent fliers seem to occupy the upper end of this range, where leading-edge separation is more likely to occur (because maximum angle of attack increases with St), but as the average flight speeds used to calculate St underestimate instantaneous speed during flapping, their true instantaneous St will be lower. Unlike bats and insects, birds have wings that are well shaped for maintaining attached flows, which offer the highest possible lift-to-drag ratios by minimizing the kinetic energy losses associated with separated flows.

Intermittent flight could further help to maintain attached flows by lowering instantaneous St, but when might this be important? Allometry implies that U should scale as $m^{1/6}$ and A as $m^{1/3}$, thus St will be scale-invariant if f scales as $m^{-1/6}$. It has been found[30] that f actually scales as $m^{-3/11}$, implying that St should scale as $m^{-7/66}$ ($m^{-0.11}$). Regressing log(St) against log(m) for the birds in our data set (Supplementary Fig. S3) confirms that St scales as roughly $m^{-0.12}$ ($n = 22$, $P = 0.003$). Constraints on wingbeat frequency may therefore mean that smaller birds have intrinsically higher St, which could make intermittent flight important for lowering St to maintain attached flows when cruising. As leading-edge separation

is probably inevitable at the very high St associated with slow flight (Fig. 2), we predict that separated flows will be normal for birds in very slow flight.

We have provided several independent confirmations that flying animals both operate within a narrow range of St when cruising and have converged on the optimum range $0.2 < St < 0.4$ expected for high propulsive efficiency and also used by cruising fish and dolphins. Cruising flight and swimming speeds therefore may be predicted as $U = fA/St$, where St ≈ 0.3. As a simple rule of thumb, a cruising animal will move at a speed just over three times the product of its stroke frequency and amplitude. Conversely, a flapping micro-air vehicle of 15-cm span cruising with a 90° stroke angle (10-cm stroke amplitude) at $10\,\mathrm{ms}^{-1}$ should attain peak propulsive efficiency at a wingbeat frequency of just over 30 Hz. Although the precise optimum St will vary with wing morphology and kinematics, this scaling seems to be general. It applies to animals moving through air and through water. It broadly applies whether the propulsion is driven by the wings or tail. It applies (in our data set) to animals ranging in size from moths to dolphins. If there are swimming or flying organisms on other planets, then we predict that it should apply to them too. □

1. Alexander, R. M. *Principles of Animal Locomotion* (Princeton Univ. Press, Princeton, 2003).
2. Rohr, J. J. *et al. Observations of Dolphin Swimming Speed and Strouhal Number.* Space and Naval Warfare Systems Center Technical Report No. 1769 (Space and Naval Warfare Systems Center, San Diego, 1998).
3. Triantafyllou, M. S., Triantafyllou, G. S. & Gopalkrishnan, R. Wake mechanics for thrust generation in oscillating foils. *Phys. Fluids A* **3**, 2835–2837 (1991).
4. Triantafyllou, G. S., Triantafyllou, M. S. & Grosenbaugh, M. A. Optimal thrust development in oscillating foils with application to fish propulsion. *J. Fluids Struct.* **7**, 205–224 (1993).
5. Triantafyllou, M. S., Triantafyllou, G. S. & Yue, D. K. P. Hydrodynamics of fishlike swimming. *Annu. Rev. Fluid Mech.* **32**, 33–53 (2000).
6. Anderson, J. M., Streitlien, K., Barrett, D. S. & Triantafyllou, M. S. Oscillating foils of high propulsive efficiency. *J. Fluid Mech.* **360**, 41–72 (1998).
7. Read, D. A., Hover, F. S. & Triantafyllou, M. S. Forces on oscillating foils for propulsion and maneuvering. *J. Fluids Struct.* **17**, 163–183 (2003).
8. Wang, Z. J. Vortex shedding and frequency selection in flapping flight. *J. Fluid Mech.* **410**, 323–341 (2000).
9. Huang, R. F., Wu, J. Y., Jeng, J. H. & Chen, R. C. Surface flow and vortex shedding of an impulsively started wing. *J. Fluid Mech.* **441**, 265–292 (2001).
10. Motani, R. Scaling effects in caudal fin propulsion and the speed of ichthyosaurs. *Nature* **415**, 309–312 (2002).
11. Bandyopadhyay, P. R., Castano, J. M., Nedderman, W. H. & Donnelly, M. J. Experimental simulations of fish-inspired unsteady vortex-dynamics on a rigid cylinder. *J. Fluids Eng.* **122**, 219–238 (2000).
12. Wolfgang, M. J., Anderson, J. M., Grosenbaugh, M. A., Yue, D. K. P. & Triantafyllou, M. S. Near-body flow dynamics in swimming fish. *J. Exp. Biol.* **202**, 2303–2327 (1999).
13. Gopalkrishnan, R., Triantafyllou, M. S., Triantafyllou, G. S. & Barrett, D. Active vorticity control in a shear flow using a flapping foil. *J. Fluid Mech.* **274**, 1–21 (1994).
14. Withers, P. C. & Timko, P. L. The significance of ground effect to the aerodynamic cost of flight and energetics of the black skimmer (*Rhyncops nigra*). *J. Exp. Biol.* **70**, 13–26 (1977).
15. Baker, P. S. & Cooter, R. J. The natural flight of the migratory locust, *Locusta migratoria L.* I. Wing movements. *J. Comp. Physiol. A* **131**, 79–87 (1979).
16. Baker, P. S., Gewecke, M. & Cooter, R. J. The natural flight of the migratory locust, *Locusta migratoria L.* III. Wing-beat frequency, flight speed and attitude. *J. Comp. Physiol.* **141**, 233–237 (1981).
17. Scholey, K. D. *Developments in Vertebrate Flight: Climbing and Gliding of Mammals and Reptiles and the Flapping Flight of Birds.* Thesis, Univ., Bristol (1983).
18. Videler, J. J., Groenewegen, A., Gnodde, M. & Vossebelt, G. Indoor flight experiments with trained kestrels II. The effect of added weight on flapping flight kinematics. *J. Exp. Biol.* **134**, 185–199 (1988).
19. Pennycuick, C. J. Span-ratio analysis used to estimate effective lift:drag ratio in the double-crested cormorant *Phalacrocorax auritus* from field observations. *J. Exp. Biol.* **142**, 1–15 (1989).
20. Dudley, R. & DeVries, P. J. Flight physiology of migrating *Urania fulgens* (*Uraniidae*) moths: kinematics and aerodynamics of natural free flight. *J. Comp. Physiol. A* **167**, 145–154 (1990).
21. Pennycuick, C. J. Predicting wingbeat frequency and wavelength of birds. *J. Exp. Biol.* **150**, 171–185 (1990).
22. Tobalske, B. W. & Dial, K. P. Neuromuscular control and kinematics of intermittent flight in budgerigars (*Melopsittacus undulatus*). *J. Exp. Biol.* **187**, 1–18 (1994).
23. Tobalske, B. W. Neuromuscular control and kinematics of intermittent flight in the European starling (*Sturnus vulgaris*). *J. Exp. Biol.* **198**, 1259–1273 (1995).
24. Pennycuick, C. J. Wingbeat frequency of birds in steady cruising flight: new data and improved predictions. *J. Exp. Biol.* **199**, 1613–1618 (1996).
25. Tobalske, B. W. Scaling of muscle composition, wing morphology, and intermittent flight behavior in woodpeckers. *Auk* **113**, 151–177 (1996).
26. Tobalske, B. W. & Dial, K. P. Flight kinematics of black-billed magpies and pigeons over a wide range of speeds. *J. Exp. Biol.* **199**, 263–280 (1996).
27. Tobalske, B. W., Peacock, W. L. & Dial, K. P. Kinematics of flap-bounding flight in the zebra finch over a wide range of speeds. *J. Exp. Biol.* **202**, 1725–1739 (1999).

28. Pennycuick, C. J. Speeds and wingbeat frequencies of migrating birds compared with calculated benchmarks. *J. Exp. Biol.* **204**, 3283–3294 (2001).
29. Bullen, R. D. & McKenzie, N. L. Scaling bat wingbeat frequency and amplitude. *J. Exp. Biol.* **205**, 2615–2626 (2002).
30. Rayner, J. M. V. Form and function in avian flight. *Curr. Ornithol.* **5**, 1–45 (1987).

....

New frog family from India reveals an ancient biogeographical link with the Seychelles

S. D. Biju[1,2]* & **Franky Bossuyt**[2]*

[1]*Tropical Botanic Garden and Research Institute, Palode, Thiruvananthapuram, 695562 Kerala, India*
[2]*Biology Department, Unit of Ecology & Systematics, Vrije Universiteit Brussel, Pleinlaan 2, B-1050 Brussels, Belgium*

* The authors contributed equally to this work

....

About 96% of the more than 4,800 living anuran species[1] belong to the Neobatrachia or advanced frogs[2–4]. Because of the extremely poor representation of these animals in the Mesozoic fossil record, hypotheses on their early evolution have to rely largely on extant taxa[5–7]. Here we report the discovery of a burrowing frog from India that is noticeably distinct from known taxa in all anuran families. Phylogenetic analyses of 2.8 kilobases of mitochondrial and nuclear DNA unambiguously designate this frog as the sister taxon of Sooglossidae, a family exclusively occurring on two granitic islands of the Seychelles archipelago[8]. Furthermore, molecular clock analyses[9] uncover the branch leading to both taxa as an ancient split in the crown-group Neobatrachia. Our discovery discloses a lineage that may have been more diverse on Indo-Madagascar in the Cretaceous period, but now only comprises four species on the Seychelles and a sole survivor in India. Because of its very distinct morphology and an inferred origin that is earlier than several neobatrachian families[10], we recognize this frog as a new family.

Amphibia L., 1758
Lissamphibia Haeckel, 1866
Anura Rafinesque, 1815
Neobatrachia Reig, 1958
Nasikabatrachidae fam. nov.
Nasikabatrachus gen. nov.
Nasikabatrachus sahyadrensis gen. et sp. nov.

Etymology. Nasika (Sanskrit) meaning nose, batrachus meaning frog, and Sahyadri, being synonymous for the Western Ghats (the hills along the west coast of the Indian subcontinent).
Holotype. Bombay Natural History Society (BNHS; Mumbai), BNHS 4202, an adult female, snout–vent length 70.1 mm, collected July 2000 by S.D.B. (Fig. 1a).
Type locality. Disturbed secondary forest near a cardamom planta-

tion at Kattappana (09° 45′ N, 77° 05′ E, altitude approximately 900 m), Idukki district, Kerala, Western Ghats, India.
Diagnosis. The diagnosis is valid for the family, genus and species. A relatively large frog with a bloated general appearance, smooth skin and an overall black coloration dorsally and dark grey ventrally; the head (Fig. 1b) is pointed and short relative to the body; the snout has a distinct white protrusion. The eyes are small with a rounded, horizontal pupil; no apparent tympanum; the forelimbs are short, the hands (Fig. 1c) are rudimentarily webbed, the tips of fingers are rounded, without disks. The hindlimbs are short, feet (Fig. 1d) are about 3/4 webbed, and the tips of toes are rounded, without disks. A large, white inner metatarsal tubercle is present on both feet (detailed measurements of external morphology are provided as Supplementary Information).

The skeleton (Fig. 1e) is characteristic of a burrowing frog and displays bones with a well-calcified cortical area, a skull with strongly ossified neurocranial and dermal elements (Fig. 1f), a short tibiale and fibulare, strong and short tibiofibular bones, and
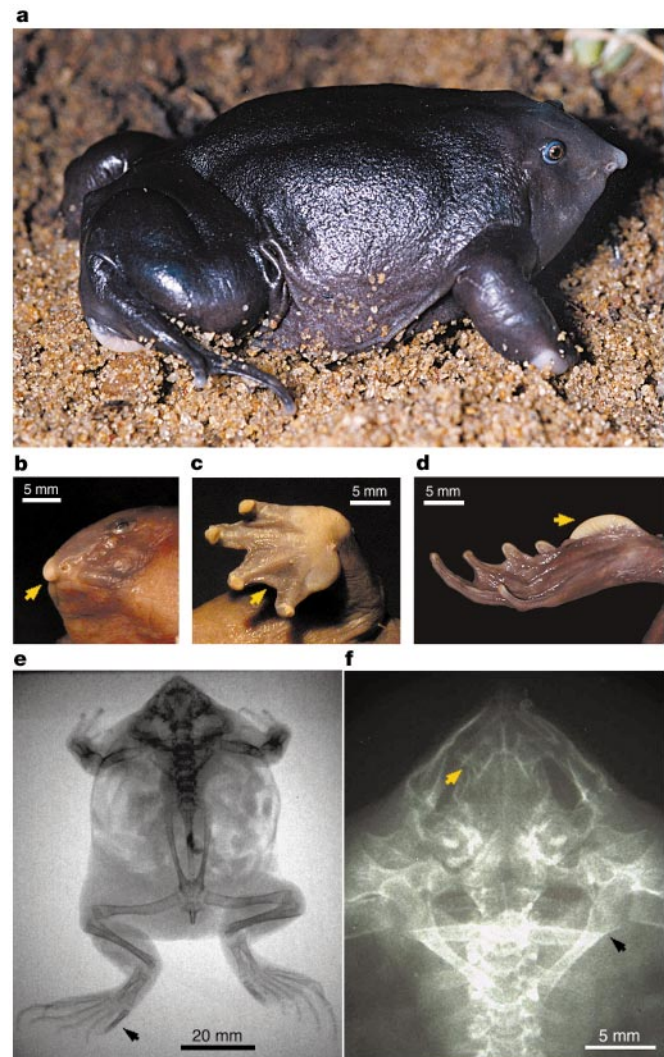

Figure 1 Holotype of *Nasikabatrachus sahyadrensis*. **a**, *Nasikabatrachus sahyadrensis* in life. **b**, Detail of head, showing slender mouth and distinct protrusion on snout. **c**, Detail of hand, showing rudimentary webbing. **d**, Detail of foot showing the large, white inner metatarsal tubercle. **e**, X-ray photograph showing strongly calcified bones. The arrow indicates the prehallux. **f**, X-ray photograph showing strongly ossified skull and pectoral girdle. The yellow arrow indicates the presumed neopalatine bone; the black arrow indicates the coracoid, the lateral end of which is wider than the medial.

© 2003 Nature Publishing Group